The 3D Galactocentric velocities of Kepler stars: marginalizing over missing RVs

RUTH ANGUS,[1,2] ADRIAN M. PRICE-WHELAN,[2] DAN FOREMAN-MACKEY,[2] JOEL ZINN,[3] AND MEGAN BEDELL[2]

[1]*Department of Astrophysics, American Museum of Natural History, 200 Central Park West, Manhattan, NY, USA*
[2]*Center for Computational Astrophysics, Flatiron Institute, 162 5th Avenue, Manhattan, NY, USA*
[3]*NSF Fellow, Department of Astrophysics, American Museum of Natural History, 200 Central Park West, Manhattan, NY, USA*

ABSTRACT

Precise Gaia measurements of positions, parallaxes, and proper motions provide an opportunity to measure the two-dimensional velocities of Milky Way stars. Where available, spectroscopic radial velocity (RV) measurements provide an opportunity to calculate *three*-dimensional stellar velocities. Gaia will provide RVs for stars as faint as the 15th magnitude in its third data release, however there are now and will remain many stars without RV measurements. Without an RV it is not possible to directly calculate 3D stellar velocities, however it is still possible to *infer* full three-dimensional stellar velocities by marginalizing over the missing RV dimension. In this paper, we calculate and infer the three-dimensional velocities of stars in the Kepler field in Galactocentric coordinates ($v_{\mathbf{x}}$, $v_{\mathbf{y}}$, $v_{\mathbf{z}}$). Where available, we use RV measurements from the Gaia, LAMOST and APOGEE spectroscopic surveys, and otherwise marginalize over missing RV measurements. Lying at a low Galactic latitude, the Kepler field is oriented close to the y-axis of the Galactocentric coordinate system. This means that, without an RV, $v_{\mathbf{y}}$ is poorly constrained but $v_{\mathbf{x}}$ and $v_{\mathbf{y}}$ can be precisely inferred. The median uncertainties on our inferred $v_{\mathbf{x}}$, $v_{\mathbf{y}}$, and $v_{\mathbf{z}}$ velocities are around 5, 17, and 5 kms^{-1}, respectively. For many applications, including kinematic age-dating, precise velocities in the $v_{\mathbf{z}}$ and $v_{\mathbf{x}}$ directions are sufficiently useful. We provide a total of 3D velocities for 178,000 stars in the Kepler field, with and without RV measurements. Although the methodology used here is broadly applicable to targets across the sky, our prior is specifically constructed from and for the Kepler field. Care should be taken to use a suitable prior when applying this method to other parts of the Galaxy.

Keywords: Milky Way Dynamics

1. INTRODUCTION

Gaia has revolutionized the field of Galactic dynamics by providing precise positions and proper motions for an unprecedented number of stars in the Milky Way. So far, Gaia has provided positions and proper motions for around 1.7 billion stars, and radial velocities (RVs) for more than 7 million stars across its 1st, 2nd and early-3rd data releases (Gaia Collaboration et al. 2016, 2018, 2020). In combination, proper motion, position, and RV measurements provide the full 3-dimensional velocity vector for any given star, which can be used to calculate its Galactic orbit. The orbits of stars can be used to date them kinematically, to explore the secular dynamical evolution of the Galaxy, to differentiate between nascent accreted stellar populations in the Milky Way's halo, and many other applications.

One of our main purposes in calculating the velocities of Kepler stars is to use Galactic kinematics to study their evolution, either by using vertical velocity dispersion as an age proxy, or by calculating their ages via an age-velocity dispersion relation (*e.g.* Angus et al. 2020; Lu et al. 2021). The ages of stars, particularly GKM stars on the main sequence, are difficult to measure because their luminosities and temperatures evolve slowly (see Soderblom 2010, for a review of stellar ages). Empirical models that relate the magnetic activity or rotation periods of stars to their age can be used to infer the ages of some low-mass dwarfs (*e.g.* Skumanich 1972; Barnes 2003, 2007; Mamajek & Hillenbrand 2008; Angus et al. 2015, 2019; Claytor et al. 2020), however, these empirical relations are often poorly calibrated for K and M dwarfs and old stars (*e.g.* Angus et al. 2015; van Saders et al. 2016, 2018; Metcalfe & Egeland 2019; Curtis et al. 2020; Spada & Lanzafame 2019; Angus et al. 2020). Galactic kinematics provides an alternative, statistical dating method. In Angus et al. (2020) we used the velocities of Kepler stars in the direction of Galactic latitude, $v_{\mathbf{b}}$ as a proxy for vertical velocity. $v_{\mathbf{b}}$ can be calculated without an RV and it is similar to $v_{\mathbf{z}}$ for many Kepler stars

because the Kepler field lies at low Galactic latitude. We used the velocity dispersions of stars as an age indicator, and used them to explore the evolution of stellar rotation rates. In Lu et al. (2021) we used *vertical* velocity dispersion to calculate kinematic ages for Kepler stars with measured rotation periods using an AVR. Those vertical velocities were inferred by marginalizing over missing RVs using the method we describe in this paper.

The star forming molecular gas clouds observed in the Milky Way have a low out-of-plane, or vertical, velocity (*e.g.* Stark & Brand 1989; Stark & Lee 2005; Aumer & Binney 2009; Martig et al. 2014; Aumer et al. 2016). In contrast, the vertical velocities of older stars are observed to be larger in magnitude on average (Strömberg 1946; Wielen 1977; Nordström et al. 2004; Holmberg et al. 2007, 2009; Aumer & Binney 2009; Casagrande et al. 2011; Ting & Rix 2019; Yu & Liu 2018). Galaxy formation simulations indicated that stars initially form from dynamically hot gas, which settles into a cooler thin disk over time during the early stages of Galactic evolution. After this initial cooling phase, giant molecular clouds and Galactic spiral arms dynamically 'reheat' the orbits of stars over time. As a result, older populations of stars have larger velocity dispersions. Regardless of the exact history of dynamical cooling and heating, the vertical velocity dispersions of thin disk stars are observed to increase with stellar age (**?**). This behavior is codified by Age-Velocity dispersion Relations (AVRs), which typically express the relationship between age and velocity dispersion as a power law: $\sigma_v \propto t^\beta$, with free parameter, β (*e.g.* Holmberg et al. 2009; Yu & Liu 2018; Mackereth et al. 2019). These expressions can be used to infer the ages of groups of stars from their velocity dispersions. However, AVRs are usually calibrated in 3D Galactocentric velocities – most commonly in v_z or W. Regardless of the coordinate system, some transformation from proper motion in RA and dec is required to calculate the kinematic ages of stars.

RV measurements, combined with positions, parallaxes, and proper motions measured in the plane of the sky, complete the full set of information needed to calculate 3D stellar velocities. However, RV can only be measured from a stellar spectrum – an observation that requires a significant number of photons and is thus expensive to obtain, particularly for faint stars. Fortunately however, Gaia proper motion measurements are of such incredible precision that, even without an RV measurement, the 3D velocity of a star can still be inferred by marginalizing over radial velocity. This will often provide a velocity that is not equally well-constrained in every direction, *i.e.* the probability density function of a star's velocity will be an oblate spheroid in 3D. In the equatorial coordinate system, a star's velocity will be tightly constrained in the directions of Right Ascension (RA) and declination, and only constrained by the prior in the radial direction. Transforming to any other coordinate system, a star's velocity probability density function will change shape via a transformation that depends on its position.

There are several applications for which the 3D velocity of a star is useful, even if its velocity is not equally well-constrained in every direction. For example, Oh et al. (2017) used Gaia proper motions to identify comoving pairs and groups of stars by marginalizing over missing RVs. In their study, the relative space motions of pairs of stars were used to establish whether they qualified as 'comoving'. In a pathological case where two stars have near identical proper motions and completely different RVs, their method would incorrectly flag them as comoving stars, however in general the Gaia proper motion precision is sufficiently high to make these cases rare.

In some cases, the velocities of stars in particular directions are more useful than others, for example, the *vertical* velocities of stars (v_z or W) are often used to study the secular orbital heating of stars in the Milky Way's disk (*e.g.* Beane et al. 2018; Yu & Liu 2018; Ting & Rix 2019; Mackereth et al. 2019). Unless the radial velocity direction precisely coincides with the vertical axis of the Milky Way, *i.e.* a star lies along the Z axis of the Galactocentric coordinate system, we can still extract some v_z information from Gaia proper motions alone. Of course, the lower the Galactic latitude of a star, the better the constraint on its v_z will be (hence why the Kepler field, located at low latitude, is particularly useful for vertical velocity studies).

AVRs are usually calibrated in Galactocentric velocity coordinates (v_x, v_y, v_z or UVW), and these velocities can only be calculated with full 6D positional and velocity information. Most Kepler stars do not currently have RV measurements. Some targets will have RVs released in Gaia's third data release, but many will not.

This paper is laid out as follows. In section 2 we describe the data used in this paper. In section 3 we describe how we calculate the kinematic ages of Kepler stars from their positions, proper motions and parallaxes, marginalizing over missing RVs. We also justify the choice of prior probability density function (PDF). In section 4 we present the 3D velocities of 178,000 Kepler stars and explore the accuracy and precision of our method.

2. THE DATA

We used the Kepler-Gaia cross-matched catalog available at gaia-kepler.fun, which includes 194764 Kepler targets, cross-matched with Gaia targets within in a 1" radius. This catalog includes Gaia positions, parallaxes, and proper motions from Gaia EDR3 and RVs from Gaia DR2. It also includes distances inferred from Gaia EDR3 parallaxes (Bailer-Jones et al. 2021). We crossmatched this catalog with the LAMOST DR5 catalog, also using a 1" radius and, where available, added APOGEE RVs from the DR16 stellar catalog (Ahumada et al. 2020). We removed stars with a Gaia parallax < 0, parallax signal-to-noise ratio < 10, or Gaia astrometric excess noise > 5. After applying these cuts our total number of targets was 178,000 stars: 28,112 with RVs from Gaia DR2, 37,567 from LAMOST DR5, and 9,955 from APOGEE DR16. In total, 54,702 stars in our sample have RVs from *either* Gaia, LAMOST, or APOGEE. The APOGEE survey has a higher spectral resolution than Gaia, which in turn is higher than LAMOST. The median RV uncertainty for stars in our sample is around 0.1 km/s for APOGEE RVs, 1 km/s for Gaia RVS, and 4 km/s for LAMOST RVs. In cases where stars had two or more available RV measurements, we adopted APOGEE RVs as a first priority, followed by Gaia, then LAMOST.

Although RVs are available for more than one in three stars in this Kepler sample, most stars with RVs are bright. Very few of the faintest stars have RV measurements because of the selection functions of spectroscopic surveys. Most of the stars in our sample with Gaia RV measurements are brighter than around 14th magnitude in Gaia G-band, and stars with LAMOST or APOGEE RVs are mostly brighter than around 16th magnitude. Figure 1 shows the apparent magnitude and temperature distributions of the stars in our sample, with and without RVs. This figure reveals the combined selection functions of the Gaia, LAMOST and APOGEE RV surveys and shows that faint stars have fewer RV measurements than bright ones.

Figure 1. The distribution of apparent Gaia magnitudes for stars in our sample with and without RV measurements from Gaia, LAMOST and APOGEE.
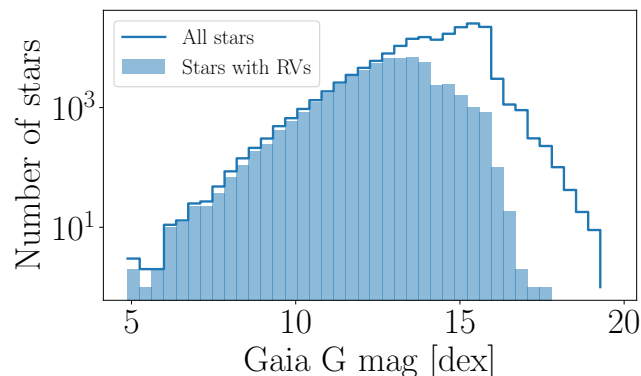

To illustrate how the populations of stars with and without RVs differ, we plot them on a color-magnitude diagram (CMD) in figure 2. The stars with RVs are generally hotter and more luminous than stars without. Most stars with RVs fall on the upper main sequence, the red giant branch, and the red clump. Most stars without RVs fall on the main sequence. This overall selection function is a combination of the APOGEE, LAMOST and Gaia DR2 selection functions.

3. METHOD

In this section we describe how we calculate full 3D velocities for stars in the Kepler field. Around 1 in 2 stars in the Kepler field have an RV from either Gaia, LAMOST, or APOGEE. For these 54,702 stars we calculated 3D velocities using the `coordinates` library of `astropy` (Astropy Collaboration et al. 2013; Price-Whelan et al. 2018). This library performs a series of matrix rotations and translations to convert stellar positions and velocities in equatorial coordinates into positions and velocities in Galactocentric coordinates. In other words, it converts positions, proper motions, parallaxes/distances, and RVs into $\mathbf{x}$, $\mathbf{y}$, $\mathbf{z}$, $v_{\mathbf{x}}$, $v_{\mathbf{y}}$, $v_{\mathbf{z}}$. For stars *without* RVs we inferred their velocities by marginalizing over their RVs using the method described below.

3.1. *Inferring 3D velocities (marginalizing over missing RV measurements)*

Figure 2. The color-temperature diagram of stars in the Kepler field with (left) and without (right) RVs provided by Gaia, LAMOST and APOGEE. The stars with RVs are generally hotter and more luminous than those without RVs, and include a large number of red clump stars and red giant branch stars. Stars without RVs are mostly concentrated on the main sequence.
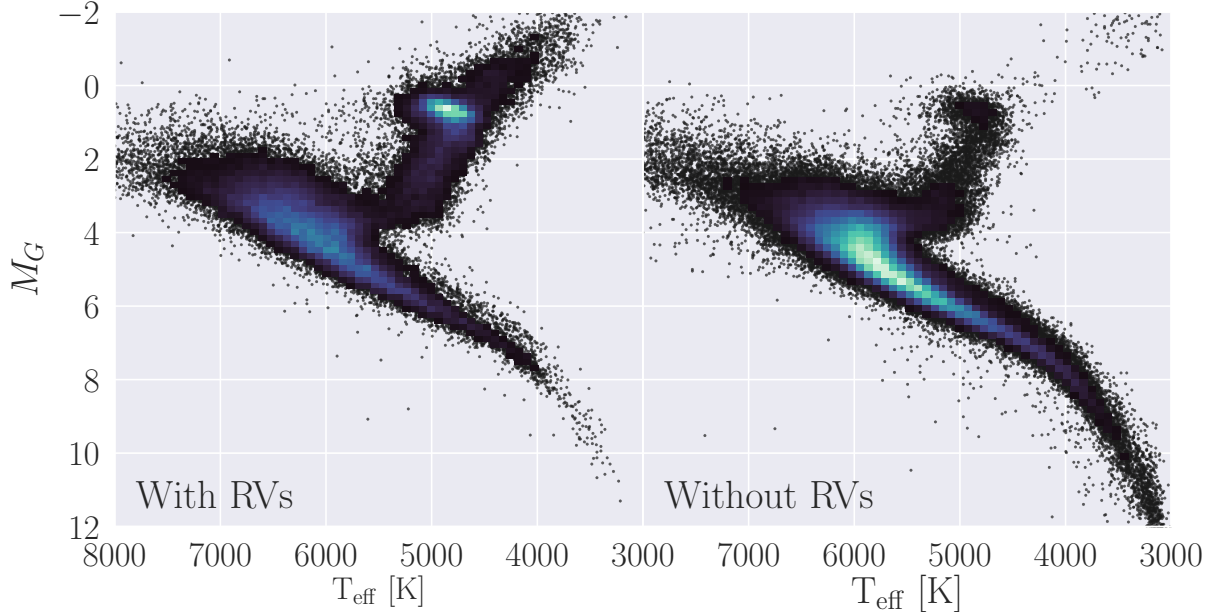
For each star in our sample without an RV measurement, we inferred $v_\mathbf{x}$, $v_\mathbf{y}$, and $v_\mathbf{z}$ from the 3D positions – RA (α), dec (δ), and parallax (π), and 2D proper motions (μ_α and μ_δ) provided in the *Gaia* EDR3 catalog (Gaia Collaboration et al. 2020). We also simultaneously inferred distance (instead of using inverse-parallax) to model velocities (see *e.g.* Bailer-Jones 2015; Bailer-Jones et al. 2018).

Using Bayes rule, the posterior probability of the velocity parameters given the Gaia data can be written:

$$p(\mathbf{v_{xyz}}, D | \mu_\alpha, \mu_\delta, \alpha, \delta, \pi) = p(\mu_\alpha, \mu_\delta, \alpha, \delta, \pi | \mathbf{v_{xyz}}, D) p(\mathbf{v_{xyz}}) p(D), \tag{1}$$

where D is distance and $\mathbf{v_{xyz}}$ is the 3D vector of velocities. To evaluate the likelihood function, our model predicts observable data from model parameters, *i.e.* it converts $v_\mathbf{x}$, $v_\mathbf{y}$ $v_\mathbf{z}$ and D to μ_α, μ_δ and π. In the first step of the model evaluation, cartesian coordinates, $\mathbf{x}$, $\mathbf{y}$, and $\mathbf{z}$ are calculated from α, δ, and D by applying a series of matrix rotations, and a translation to account for the Solar position. The cartesian Galactocentric velocity parameters, $v_\mathbf{x}$, $v_\mathbf{y}$, and $v_\mathbf{z}$, are then converted to equatorial coordinates, μ_α and μ_δ via another rotation. The posterior PDFs of the parameters $v_\mathbf{x}$, $v_\mathbf{y}$, $v_\mathbf{z}$, and $\ln(D)$ are sampled by evaluating this model over a range of parameter values which are chosen by via the No U-Turns Sampler (NUTS) algorithm in `PyMC3`. At each set of model parameters the likelihood is calculated via a Gaussian likelihood function, and multiplied by a prior (described below) to produce the posterior probability: the probability of those model parameters given the data.

For computational efficiency, we used `PyMC3` to sample the posterior PDFs of stellar velocities (Salvatier et al. 2016). This required that we rewrite the `astropy` coordinate transformation code using `numpy` and `Theano` (Harris et al. 2020; The Theano Development Team et al. 2016). The series of rotations and translations required to convert from equatorial to Galactocentric coordinates is described in the astropy documentation[1]. For each star in the Kepler field, we explored the posteriors of the four parameters, $v_\mathbf{x}$, $v_\mathbf{y}$, $v_\mathbf{z}$, and $\ln(D)$ using the *PyMC3* No U-Turn Sampler (NUTS) algorithm, and the `exoplanet` *Python* library (Foreman-Mackey & Barentsen 2019). We tuned the *PyMC3* sampler for 1500 steps, with a target acceptance fraction of 0.9, then ran four chains of 1000 steps for a total of 4000 steps. This resulted in a $\hat{r}$-statistic (the ratio of intra-chain to inter-chain variance) of around unity, indicating convergence. Using PyMC3 made this inference procedure exceptionally fast – taking just a few seconds per star on a laptop.

---

[1] https://docs.astropy.org/en/stable/coordinates/galactocentric.html

3.2. *The prior*

As mentioned previously, the positioning of the Kepler field at low Galactic latitude allows $v_{\mathbf{z}}$ to be well-constrained from proper motion measurements alone. This also happens to be the case for $v_{\mathbf{x}}$, because the direction of the Kepler field is almost aligned with the **y**-axis of the Galactocentric coordinate system and is almost perpendicular to both the **x** and **z**-axes (see figure 3). For this reason, the **y**-direction is similar to the radial direction for observers near the Sun, so $v_{\mathbf{y}}$ will be poorly constrained for Kepler stars without RV measurements. On the other hand, $v_{\mathbf{x}}$ and $v_{\mathbf{z}}$ are almost perpendicular to the radial direction and can be precisely inferred with proper motions alone.

Figure 3. **x**, **y** and **z** positions of stars observed by Kepler, showing the orientation of the Kepler field. The direction of the field is almost aligned with the **y**-axis and almost perpendicular to the **x** and **z**-axes, which is why $v_{\mathbf{x}}$ and $v_{\mathbf{z}}$ can be tightly constrained for Kepler stars without RVs, but $v_{\mathbf{y}}$ cannot.
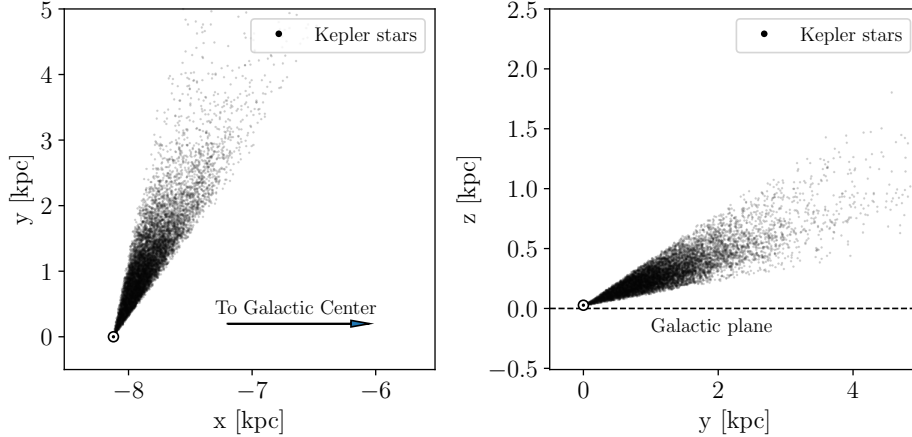

We constructed a multivariate Gaussian prior PDF over distance and 3D velocity using the Kepler targets *which have RV measurements*. We calculated the means and covariances of the $v_{\mathbf{x}}$, $v_{\mathbf{y}}$, $v_{\mathbf{z}}$ and $\ln(D)$ distributions of stars with measured RVs and then used these means and covariances to construct a multivariate Gaussian prior over the velocity and distance parameters for stars *without* RVs. Velocity outliers greater than 3-σ were removed before calculating the means and covariances of the distributions. The distance and velocity distributions of Kepler targets with RVs are displayed in figure 4. These are the distributions we used to construct the prior. The 2-σ contour of the multivariate Gaussian prior is shown in each panel as a black ellipse.

Our goal was to infer the velocities of stars *without* RV measurements using a prior calculated from stars *with* RV measurements. However, stars with and without RVs are likely to be quite different populations, determined by the Gaia, LAMOST and APOGEE selection functions. In particular, stars without RV measurements are more likely to be fainter, less luminous, cooler and potentially older. Figure 2 shows the populations of stars with and without RVs on the CMD – stars with RVs are more likely to be upper-main-sequence and red giant stars, and stars without RVs are more likely to be mid and lower main-sequence dwarfs. For this reason, a prior based on the velocity distributions of stars *with* RVs will not necessarily reflect the velocities of those without.

We tested the influence of the prior on the velocities we inferred. One of the main features of the RV selection functions is brightness: Gaia DR2 RVs are only available for stars brighter than around 14th magnitude, and LAMOST DR5 and APOGEE DR16 RVs for stars brighter than around 16th magnitude. For this reason, we tested priors based on stellar populations with different apparent magnitudes. Three priors were tested: one calculated from the velocity distributions of the brightest half of the RV sample (*Gaia G*-band apparent magnitude < 13), one from the faintest half ($G > 13$), and one from *all* stars with RVs. Figure 5 shows the distributions of the faint (blue) and bright (orange) halves of the RV sample as kernel density estimates (KDEs). The distributions are different because bright stars are typically more massive, younger, more evolved, and/or closer to the Sun on average than faint stars. As a result, these stars occupy slightly different Galactic orbits. The multivariate Gaussian, fit to these distributions, which was used as a prior PDF, is shown as single-dimension projections in figure 5. The Gaussian fit to the bright and faint star distributions are shown as dashed orange and blue lines, respectively. The Gaussian fit to *all* the data, both bright and faint, is shown as a black solid line. The means of the faint and bright distributions differ by 6 kms^{-1}, 5 kms^{-1}, 1

Figure 4. The 2D velocity and distance distributions for stars with RV measurements, used to construct a multivariate Gaussian prior over velocity and distance parameters for stars *without* RVs. 2-σ contours are shown in blue.
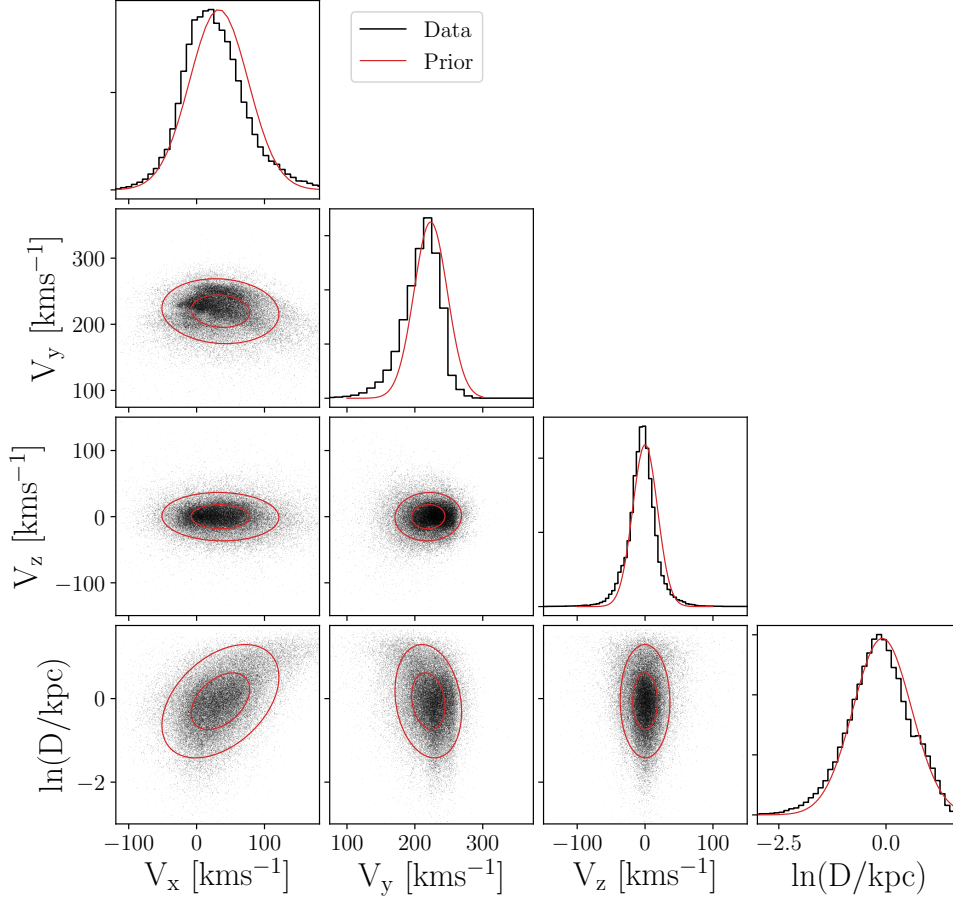
kms^{-1} and 0.21 kpc, for $v_{\mathbf{x}}$ $v_{\mathbf{y}}$, $v_{\mathbf{z}}$ and $\ln(D)$, respectively. The $v_{\mathbf{x}}$, $v_{\mathbf{y}}$, and distance distributions of the bright stars are slightly non-Gaussian – more so than the faint stars. This highlights the inadequacy of using a Gaussian distribution as the prior – a Gaussian is only an approximation of the underlying distribution of stars in our sample. As a result of this approximation, inferred velocities that are strongly prior-dependent – (*i.e.*especially those in the **y**-direction) may inherit some inaccuracies from the Gaussian prior, which is not a perfect representation of the underlying data. However, given that the populations of stars with and without RV measurements are different, it may be inappropriate to use a more complex, more informative prior anyway.

We inferred the velocities of 3000 stars chosen at random from the RV Kepler sample using each of these three priors and compared the inferred velocity distributions. If the inferred velocities were highly prior-dependent, the resulting distributions, obtained from different priors, would look very different. The results of this test are shown in figure 6. From left to right, the three panels show the distributions of inferred $v_{\mathbf{x}}$, $v_{\mathbf{y}}$, and $v_{\mathbf{z}}$. The blue dashed line shows a KDE, representing the distributions of velocities inferred using the prior calculated from the faint half of the RV sample. Similarly, the solid orange line shows the distribution of inferred velocities using the prior calculated from the bright half of the RV sample, and the solid black line shows the results of the prior calculated from *all* stars with measured RVs.

Figure 5. Velocity and distance distributions of faint (blue) and bright (orange) stars with RVs, shown as KDEs. Gaussian fits to these distributions are shown as dashed lines in corresponding colors. The solid black line shows the Gaussian fit to all data (bright and faint combined) and is the prior we ended up using in our model.
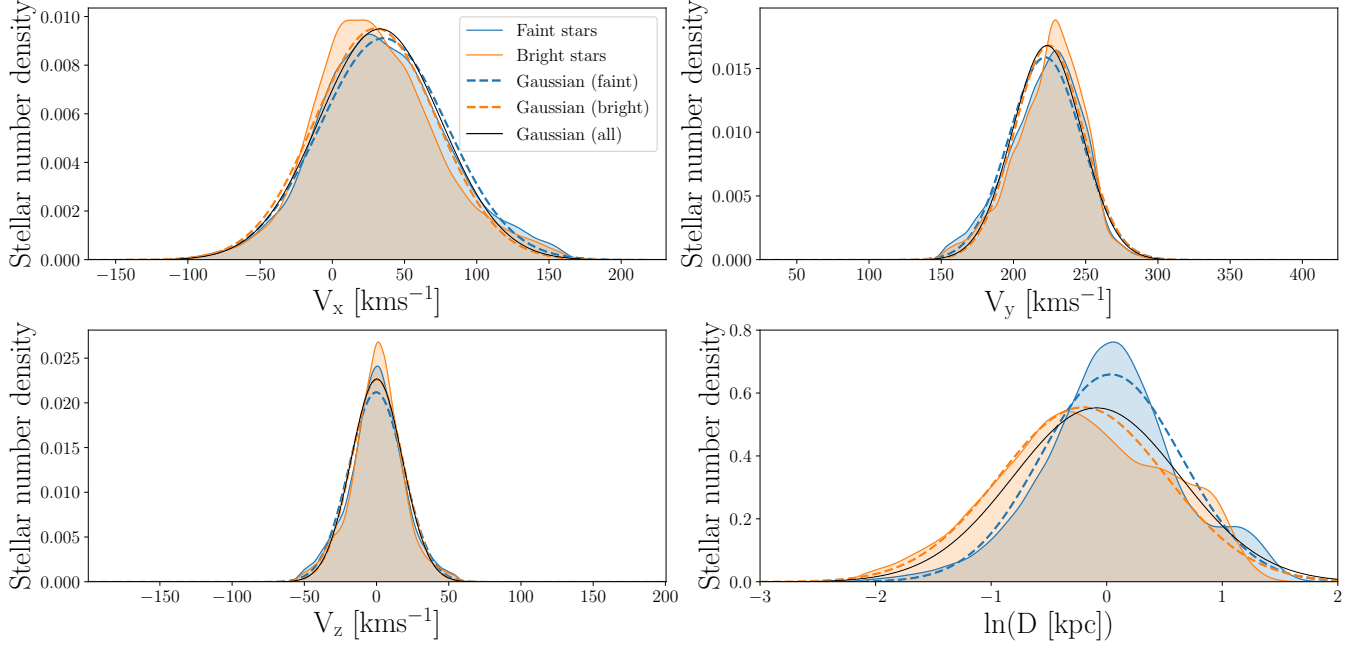
The median values of the $v_{\mathbf{y}}$ distributions, resulting from the faint and bright priors, differ by around 4 kms^{-1}. This is similar to the difference in means of the faint and bright populations (5 kms^{-1}, as quoted above). The inferred $v_{\mathbf{x}}$ and $v_{\mathbf{z}}$ distributions differ by 2 kms^{-1} and 0.3 kms^{-1}, respectively. Regardless of the prior choice, the $v_{\mathbf{x}}$ and $v_{\mathbf{z}}$ distributions are similar because velocities in the $\mathbf{x}$ and $\mathbf{z}$-directions are not strongly prior dependent: they are tightly constrained with proper motion measurements alone. However, the distribution of inferred $v_{\mathbf{y}}$ velocities *does* depend on the prior. This is because the $\mathbf{y}$-direction is close to the radial direction for Kepler stars (see figure 3), and $v_{\mathbf{y}}$ cannot be tightly constrained without an RV measurement.

Figure 6. The distributions of velocity and distance parameters, inferred using three different priors. The orange line is a KDE that represents the distribution of parameters inferred with a Gaussian prior, estimated from the bright half of the RV sample ($G < 13.9$). The blue dashed line shows the results from a prior estimated from the faint half of the RV sample ($G > 13.9$. The black line shows the results from a prior calculated from all stars with RV measurements and is the prior we adopt in our final analysis.
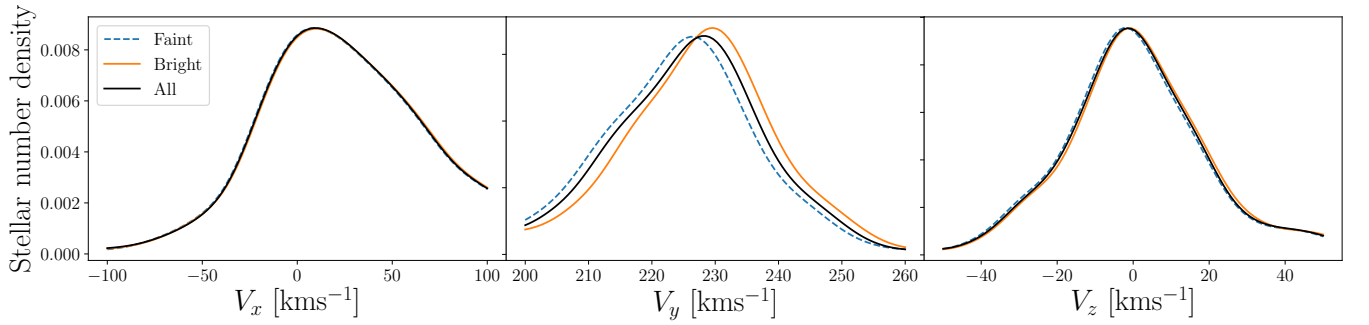
Although this test was performed on stars with RV measurements, which are brighter overall than the sample of stars without RVs (*e.g.* figure 1), figure 6 nevertheless shows that $v_{\mathbf{x}}$ and $v_{\mathbf{z}}$ are not strongly prior-dependent. Since

this work is chiefly motivated by kinematic age-dating, which mostly requires vertical velocities, $v_{\mathbf{z}}$ we are satisfied with these results. The difference in the dispersions of $v_{\mathbf{z}}$ velocities, calculated with the three different priors tested above was smaller than 0.5 kms^{-1}. We conclude that the $v_{\mathbf{x}}$ and $v_{\mathbf{z}}$ velocities we infer are relatively insensitive to prior choice, and we adopt a prior calculated from the distributions of all stars with RV measurements (black Gaussians in figure 5). The $v_{\mathbf{y}}$ velocities are more strongly prior dependent and should be used with caution.

4. RESULTS

4.1. *Inferred velocities*

Figure 7 shows the inferred velocities of 5000 randomly selected Kepler stars. The 2D distributions of inferred stellar velocities are plotted in the lower-left panels, with black contours indicating the stellar number density. The orange contours in these panels show the marginal projections of the Gaussian prior in 2D. The upper right panels in the figure, lying on the diagonal plot, show the 1D distributions (histograms) of stellar velocities. The black histogram shows the distribution of inferred velocities, the blue histogram shows the distribution of velocities calculated for stars with RVs, and the orange lines show the 1D marginal Gaussian prior distributions. This figure shows that the velocity distributions of stars calculated with and without RVs are broadly similar. The prior distribution is calculated using the velocities of stars with RVs. If the velocity distributions of stars were Gaussian, the 1D orange Gaussians would look like the blue histograms. In other words, the differences between the orange lines and blue histograms is caused by the non-Gaussianity of the velocity distributions.

Among stars with measured RVs, $v_{\mathbf{y}}$ and $v_{\mathbf{z}}$ are slightly positively correlated: stars with larger $v_{\mathbf{y}}$ tend to have larger $v_{\mathbf{z}}$. However, the inferred velocities have the opposite trend: stars with larger $v_{\mathbf{y}}$ have a smaller $v_{\mathbf{z}}$. This difference is caused by the slight degeneracy between $v_{\mathbf{y}}$ and $v_{\mathbf{z}}$ for stars that do not have RVs. The proper motions of stars with a given $v_{\mathbf{y}}$ and $v_{\mathbf{z}}$ could be equally well-described with a slightly larger $v_{\mathbf{y}}$ and a smaller $v_{\mathbf{z}}$ or vice versa.

To validate our method, we inferred velocities for stars in our sample with measured RVs and compared those inferred values with velocities calculated directly from 6D position, proper motion, and RV measurements. Figure 8 shows the $v_{\mathbf{x}}$, $v_{\mathbf{y}}$ and $v_{\mathbf{z}}$ velocities we inferred, for 3000 stars chosen at random, compared with those calculated from measured RVs.

The three velocity components, $v_{\mathbf{x}}$, $v_{\mathbf{y}}$ and $v_{\mathbf{z}}$ were recovered with differing levels of precision: $v_{\mathbf{x}}$ and $v_{\mathbf{z}}$ are inferred more precisely than $v_{\mathbf{y}}$. This is because of the orientation of the Kepler field, shown in figure 3. Slight inaccuracies seen in the residual panels for $v_{\mathbf{x}}$ and $v_{\mathbf{z}}$ are caused by .... Quote some summary statistics.

Table ?? contains the inferred 3D velocities of stars in our sample, in addition to their positional and velocity information from Gaia EDR3, LAMOST DR5 and APOGEE DR16. A sample of this table is displayed here, and the full machine-readable table is available online.

5. CONCLUSION

This paper describes a method for inferring the 3D velocities of stars by marginalizing over missing radial velocity measurements. We focused on stars in the Kepler field, because of its potential for studying stellar evolution via kinematic age-dating, and because of its particular orientation. Located at low Galactic latitude, the Kepler field is almost aligned with the y-axis of the Galactocentric coordinate system. This means that 2D Gaia proper motion measurements alone are sufficient to tightly constrain the $v_{\mathbf{x}}$ and $v_{\mathbf{z}}$ velocities of Kepler stars. Without RV measurements however, the $v_{\mathbf{y}}$ velocities of Kepler stars are poorly constrained. However, given that many age-velocity dispersion relations (AVR) are calibrated in *vertical* velocity, $v_{\mathbf{z}}$ is the main parameter of interest for kinematic age-dating.

We compiled crossmatches of the Kepler, Gaia EDR3, LAMOST DR5 and APOGEE DR16 catalogs. Gaia EDR3 provided parallaxes, positions and proper motions for the stars in our sample, and Gaia DR2 provided RVs for XXX stars. LAMOST DR5 provided XXX RVs for stars in our sample, and APOGEE DR16 provided XXX. Of the three spectroscopic surveys, APOGEE has the highest resolution, followed by Gaia, then LAMOST, so we adopted RVs in that priority-order where stars had multiple RV measurements available.

We calculated $v_{\mathbf{x}}$, $v_{\mathbf{y}}$, and $v_{\mathbf{z}}$ for the XXX stars in our sample with RVs using `astropy`. For the remaining XXX stars, we *inferred* $v_{\mathbf{x}}$, $v_{\mathbf{y}}$, $v_{\mathbf{z}}$, and distance while marginalizing over RV. Our prior was a 4D Gaussian in $v_{\mathbf{x}}$, $v_{\mathbf{y}}$, $v_{\mathbf{z}}$ and ln(distance), which was based on the distribution of stars in our sample *with* RVs. Since the populations of stars with and without RVs in the Kepler field are somewhat different – stars *with* RVs are generally brighter than stars without – we tested the sensitivity of our results to the prior. We split the subsample of stars with measured RVs into two further subgroups: stars brighter and stars fainter than 13th magnitude in Gaia G-band (13th being the median

Figure 7. The distribution of inferred stellar velocities and distances. Figure 7 shows the inferred velocities of 5000 randomly selected Kepler stars. The 2D distributions of inferred stellar velocities are plotted in the lower-left panels, with black contours indicating the stellar number density. The orange contours in the lower-left panels show the marginal projections of the Gaussian prior distribution in 2D. The upper-right panels in the figure, lying on the plot's diagonal, show the 1D distributions (histograms) of stellar velocities. The black histogram shows the distribution of inferred velocities, the blue histogram shows the distribution of velocities for stars with RVs, and the orange lines show the 1D marginal Gaussian prior distributions.
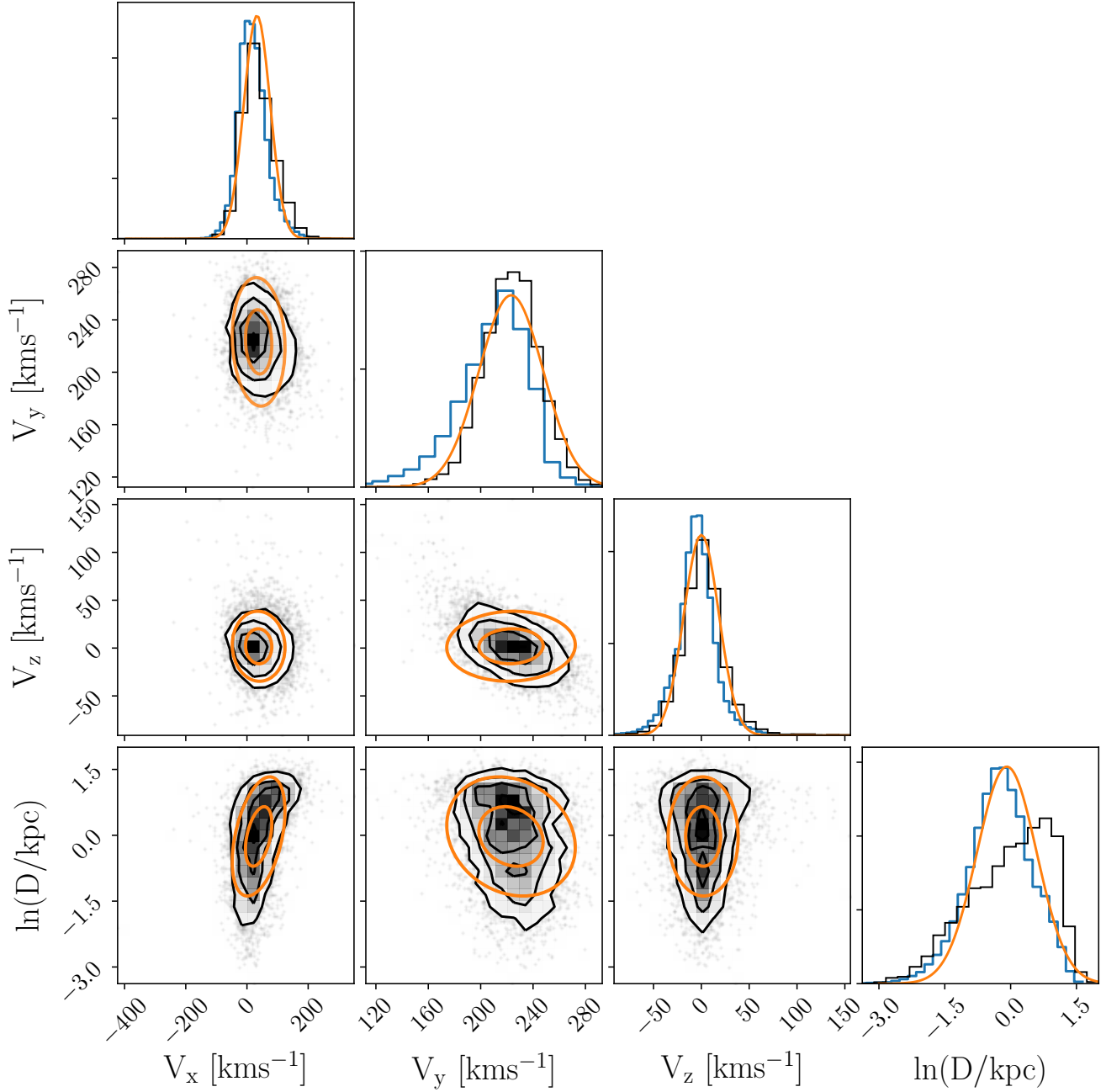
magnitude of the Kepler stars with RVs). Priors were constructed from the faint and bright halves of the sample and used to infer the velocities of 1000 stars randomly selected from the total RV sample. Upon examination, we found the final inferred velocities were similar, irrespective of the prior. As expected, v_x and v_z depend very little on the prior

Figure 8. Vertical velocities calculated with full 6D information vs vertical velocities inferred without RVs, for 3000 Kepler targets with RV measurements.
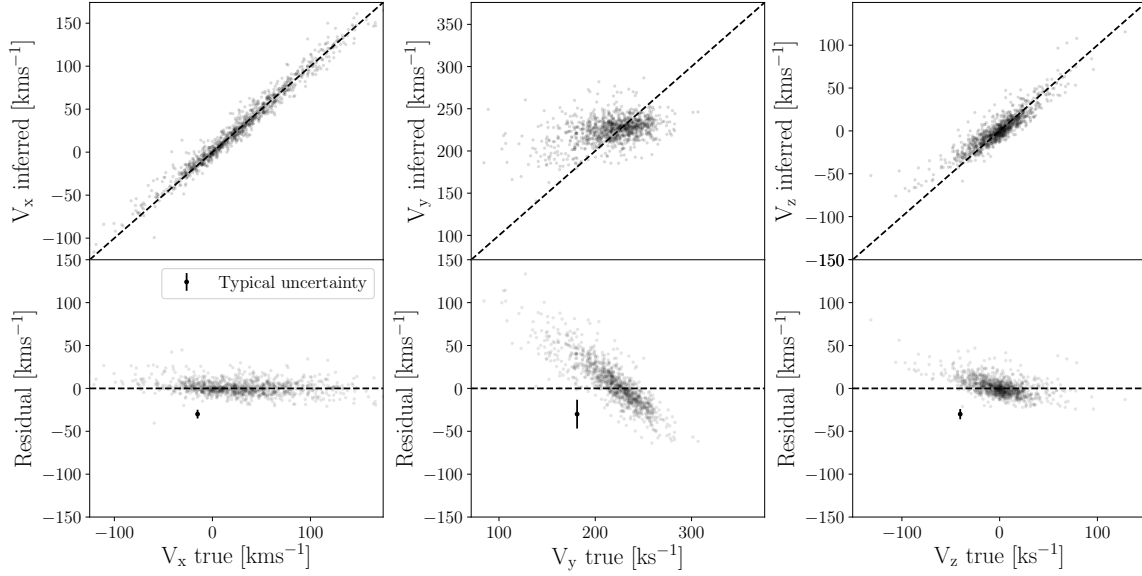
but $v_{\mathbf{y}}$ has a stronger prior-dependence because it is difficult to constrain without an RV for Kepler stars. A caveat of our inferred velocities is therefore that the $v_{\mathbf{y}}$ velocities may not be accurate for faint stars in the Kepler field.

We provide a table of $v_{\mathbf{x}}$, $v_{\mathbf{y}}$, $v_{\mathbf{z}}$, and ln(distance) for a total of XXX stars observed by Kepler. This table also contains the positional and velocitiy information from Gaia DR2, Gaia EDR3, LAMOST DR5, and APOGEE DR16.

This work made use of the gaia-kepler.fun crossmatch database created by Megan Bedell.

Some of the data presented in this paper were obtained from the Mikulski Archive for Space Telescopes (MAST). STScI is operated by the Association of Universities for Research in Astronomy, Inc., under NASA contract NAS5-26555. Support for MAST for non-HST data is provided by the NASA Office of Space Science via grant NNX09AF08G and by other grants and contracts. This paper includes data collected by the Kepler mission. Funding for the Kepler mission is provided by the NASA Science Mission directorate.

This work has made use of data from the European Space Agency (ESA) mission *Gaia* (https://www.cosmos.esa.int/gaia), processed by the *Gaia* Data Processing and Analysis Consortium (DPAC, https://www.cosmos.esa.int/web/gaia/dpac/consortium). Funding for the DPAC has been provided by national institutions, in particular the institutions participating in the *Gaia* Multilateral Agreement.

REFERENCES

Ahumada, R., Prieto, C. A., Almeida, A., & *et al.* 2020, ApJS, 249, 3, doi: 10.3847/1538-4365/ab929e

Angus, R., Aigrain, S., & Foreman-Mackey *et al*, D. 2015, MNRAS, 450, 1787, doi: 10.1093/mnras/stv423

Angus, R., Morton, T. D., & Foreman-Mackey *et al*, D. 2019, AJ, 158, 173, doi: 10.3847/1538-3881/ab3c53

Angus, R., Beane, A., Price-Whelan, A. M., et al. 2020, AJ, 160, 90, doi: 10.3847/1538-3881/ab91b2

Astropy Collaboration, Robitaille, T. P., & Tollerud *et al*, E. J. 2013, A&A, 558, A33, doi: 10.1051/0004-6361/201322068

Aumer, M., Binney, J., & Schönrich, R. 2016, MNRAS, 462, 1697, doi: 10.1093/mnras/stw1639

Aumer, M., & Binney, J. J. 2009, MNRAS, 397, 1286, doi: 10.1111/j.1365-2966.2009.15053.x

Bailer-Jones, C. A. L. 2015, PASP, 127, 994, doi: 10.1086/683116

Bailer-Jones, C. A. L., Rybizki, J., Fouesneau, M., Demleitner, M., & Andrae, R. 2021, AJ, 161, 147, doi: 10.3847/1538-3881/abd806

Bailer-Jones, C. A. L., Rybizki, J., & Fouesneau *et al*, M. 2018, AJ, 156, 58, doi: 10.3847/1538-3881/aacb21

Barnes, S. A. 2003, ApJ, 586, 464, doi: 10.1086/367639

—. 2007, ApJ, 669, 1167, doi: 10.1086/519295

Beane, A., Ness, M. K., & Bedell, M. 2018, ApJ, 867, 31, doi: 10.3847/1538-4357/aae07f

Casagrande, L., Schönrich, R., & Asplund *et al*, M. 2011, A&A, 530, A138, doi: 10.1051/0004-6361/201016276

Claytor, Z. R., van Saders, J. L., Santos, Â. R. G., et al. 2020, ApJ, 888, 43, doi: 10.3847/1538-4357/ab5c24

Curtis, J. L., Agüeros, M. A., Matt, S. P., et al. 2020, ApJ, 904, 140, doi: 10.3847/1538-4357/abbf58

Foreman-Mackey, D., & Barentsen, G. 2019, dfm/exoplanet: exoplanet v0.1.3, v0.1.3, Zenodo, doi: 10.5281/zenodo.2536576

Gaia Collaboration, Brown, A. G. A., Vallenari, A., et al. 2020, arXiv e-prints, arXiv:2012.01533. https://arxiv.org/abs/2012.01533

Gaia Collaboration, Brown, A. G. A., Vallenari, A., & Prusti, T. *et al.* 2018, A&A, 616, A1, doi: 10.1051/0004-6361/201833051

Gaia Collaboration, Prusti, T., de Bruijne, J. H. J., & Brown, A. G. A. *et al.*. 2016, A&A, 595, A1, doi: 10.1051/0004-6361/201629272

Harris, C. R., Millman, K. J., van der Walt, S. J., et al. 2020, Nature, 585, 357, doi: 10.1038/s41586-020-2649-2

Holmberg, J., Nordström, B., & Andersen, J. 2007, A&A, 475, 519, doi: 10.1051/0004-6361:20077221

—. 2009, A&A, 501, 941, doi: 10.1051/0004-6361/200811191

Lu, Yuxi, Angus, R., et al. 2021, arXiv e-prints, arXiv:2102.01772. https://arxiv.org/abs/2102.01772

Mackereth, J. T., Bovy, J., Leung, H. W., et al. 2019, MNRAS, 489, 176, doi: 10.1093/mnras/stz1521

Mamajek, E. E., & Hillenbrand, L. A. 2008, ApJ, 687, 1264, doi: 10.1086/591785

Martig, M., Minchev, I., & Flynn, C. 2014, MNRAS, 443, 2452, doi: 10.1093/mnras/stu1322

Metcalfe, T. S., & Egeland, R. 2019, ApJ, 871, 39, doi: 10.3847/1538-4357/aaf575

Nordström, B., Mayor, M., & Andersen *et al*, J. 2004, A&A, 418, 989, doi: 10.1051/0004-6361:20035959

Oh, S., Price-Whelan, A. M., Hogg, D. W., Morton, T. D., & Spergel, D. N. 2017, AJ, 153, 257, doi: 10.3847/1538-3881/aa6ffd

Price-Whelan, A. M., Sipőcz, B. M., & Günther *et al*, H. M. 2018, AJ, 156, 123, doi: 10.3847/1538-3881/aabc4f

Salvatier, J., Wiecki, T. V., & Fonnesbeck, C. 2016, PyMC3: Python probabilistic programming framework. http://ascl.net/1610.016

Skumanich, A. 1972, ApJ, 171, 565, doi: 10.1086/151310

Soderblom, D. R. 2010, ARA&A, 48, 581, doi: 10.1146/annurev-astro-081309-130806

Spada, F., & Lanzafame, A. C. 2019, arXiv e-prints, arXiv:1908.00345. https://arxiv.org/abs/1908.00345

Stark, A. A., & Brand, J. 1989, ApJ, 339, 763, doi: 10.1086/167334

Stark, A. A., & Lee, Y. 2005, ApJL, 619, L159, doi: 10.1086/427936

Strömberg, G. 1946, ApJ, 104, 12, doi: 10.1086/144830

The Theano Development Team, Al-Rfou, R., Alain, G., et al. 2016, arXiv e-prints, arXiv:1605.02688. https://arxiv.org/abs/1605.02688

Ting, Y.-S., & Rix, H.-W. 2019, ApJ, 878, 21, doi: 10.3847/1538-4357/ab1ea5

van Saders, J. L., Ceillier, T., & Metcalfe *et al*, T. S. 2016, Nature, 529, 181, doi: 10.1038/nature16168

van Saders, J. L., Pinsonneault, M. H., & Barbieri, M. 2018, ArXiv e-prints. https://arxiv.org/abs/1803.04971

Wielen, R. 1977, A&A, 60, 263

Yu, J., & Liu, C. 2018, MNRAS, 475, 1093, doi: 10.1093/mnras/stx3204